Received: 21 September 2024 | Revised: 27 November 2024 | Accepted: 16 December 2024

DOI: 10.1111/jeu.13074

Journal of Eukaryotic Microbiology ISOP Published by the International Society of Protistologists

ORIGINAL ARTICLE

Ultrastructure of *Olkasia polycarbonata* (Euglenozoa, Euglenida) demonstrates cytoskeletal innovations associated with the feeding and flagellar apparatuses

Maia V. Palka[1] | **Regine Claire Manglicmot**[2] | **Gordon Lax**[1] | **Kevin C. Wakeman**[3,4] | **Brian S. Leander**[1,2]

[1]Department of Botany, University of British Columbia, Vancouver, British Columbia, Canada

[2]Department of Zoology, University of British Columbia, Vancouver, British Columbia, Canada

[3]Institute for the Advancement of Higher Education, Hokkaido University, Sapporo, Hokkaido, Japan

[4]Graduate School of Science, Hokkaido University, Sapporo, Hokkaido, Japan

Correspondence
Maia V. Palka, Department of Botany, University of British Columbia, 6270 University Blvd., Vancouver, BC V6T 1Z4, Canada.
Email: maia.palka@gmail.com

Funding information
Natural Sciences and Engineering Research Council of Canada, Grant/Award Number: 2019-03986; Japanese Society for the Promotion of Science, Grant/Award Number: 18K14774

Abstract

Euglenids are flagellates with diverse modes of nutrition, including the photosynthetic Euglenophyceae, which acquired plastids via secondary endosymbiosis with green algae, and a diverse assemblage of predators of bacteria and other microeukaryotes. Most heterotrophic euglenids have never been cultivated, so their morphology remains poorly characterized and limited to only a few studies. "Ploeotids" are a paraphyletic group representing much of the diversity of heterotrophic euglenids and are characterized by their feeding apparatus and a rigid pellicle of 10–12 longitudinally arranged strips. Ploeotid-like euglenids gave rise to the Spirocuta, a large clade of heterotrophic and photosynthetic euglenids defined by a flexible pellicle of helically arranged strips. Using single-cell approaches, we report the first ultrastructural characterization of *Olkasia polycarbonata*, a ploeotid that is consistently positioned as the sister lineage to the Spirocuta in multigene phylogenetic analyses. *O. polycarbonata* shares several morphological characteristics with members of Spirocuta, such as prominent swellings on the paraxonemal rods and a robust feeding apparatus consisting of rods and vanes. These morphological traits are consistent with the phylogenetic position of *O. polycarbonata* and demonstrate an increase in cytoskeletal complexity that occurred prior to the key strip duplication event in the most recent common ancestor of Spirocuta.

KEYWORDS
18S rDNA, Euglenozoa, extrusomes, feeding rods, flagellar roots, microtubules, paraxonemal rod, pellicle strips, *Ploeotia*, Spirocuta

INTRODUCTION

EUGLENOZOANS (Discoba) form a clade of diverse microbial eukaryotes that consists of four distinct subgroups: (1) kinetoplastids, (2) diplonemids, (3) symbiontids, and (4) euglenids (Lax et al., 2021; Leander et al., 2017). Kinetoplastids include not only the human pathogens *Trypanosoma* and *Leishmania* but also free-living lineages (Kostygov et al., 2021). Diplonemids are small, flagellated organisms, some of which are abundant in the marine pelagic zone, although they are still poorly characterized (David & Archibald, 2016; Kostygov et al., 2021). Symbiontids are found in low-oxygen marine environments, share traits associated with the presence of episymbiotic bacteria, and form an independent branch within the Euglenozoa in multigene phylogenetic analyses (Breglia et al., 2010; Lax et al., 2021; Simpson et al., 1997; Yubuki et al., 2009). Euglenids comprise

flagellates with distinctive cytoskeletal traits (e.g. pellicle strips) associated with diverse modes of nutrition and locomotion and inhabit marine, soil, and freshwater environments (Leander et al., 2017). This clade includes a lineage that acquired photosynthesis via a secondary endosymbiotic event with green algal prey cells and heterotrophic lineages that are predators of bacteria and other eukaryotes (Leander, 2004; Leander et al., 2007, 2017). Unlike most photosynthetic and osmotrophic lineages of euglenids that swim in the water column, the phagotrophic lineages glide along substrates using their dorsal flagellum, their ventral flagellum, or both (Leander, 2004; Leander et al., 2017).

Phototrophic euglenids comprise a distinct clade, the Euglenophyceae, characterized by green secondary plastids and the ability to sense light using an apparatus consisting of an orange shading structure called the "stigma" (also called the eyespot), an expanded flagellar pocket called the "reservoir" and a photosensory swelling (syn., paraxonemal body) positioned at the base of the emergent dorsal flagellum (Kuznicki et al., 1990; Leander, 2004; Leander et al., 2017). Many phototrophic and osmotrophic species have been cultivated, and consequently, the diversity and ultrastructural traits of these lineages have been relatively well studied (Lax et al., 2019; Leander et al., 2017). In contrast, the vast majority of phagotrophic euglenids have never been cultivated but can be investigated using cultivation-independent techniques, like single-cell isolations, for further study (Lax et al., 2019, 2021). Therefore, the ultrastructure of phagotrophic euglenids remains poorly understood and detailed studies are limited to a small number of studied taxa, such as *Peranema trichophorum*, *Serpenomonas costata, Entosiphon sulcatum, Neometanema parovale*, *Notosolenus urceolatus*, and *Teloprocta scaphurum* (Breglia et al., 2013; Leander, Triemer, & Farmer, 2001; Lee & Simpson, 2014a; Lee & Simpson, 2014b; Linton & Triemer, 1999; Solomon et al., 1987; Triemer & Fritz, 1987; Triemer, 1997). Despite this limited sampling, what is known about the ultrastructure of phagotrophic euglenids demonstrates a complex and exceptionally diverse suite of traits associated with their feeding and flagellar apparatuses (Leander et al., 2007, 2017; Leander, Triemer, & Farmer, 2001). There are also poorly understood ultrastructural characters that have only been observed in a few representative taxa, such as the flagellar swellings observed in *Urceolus cyclostomus* and *N. parovale* (Leander, Triemer, & Farmer, 2001; Lee & Simpson, 2014a, 2014b). This structural diversity is intimately associated with the diverse modes of feeding and locomotion observed across euglenids. The large degree of variation in the structure and organization of euglenid cytoskeletons described so far in a relatively limited number of taxa illustrates the need for further ultrastructural studies of phagotrophic species to better understand their diversity and evolutionary history.

The euglenid feeding apparatus is a diverse cytoskeletal system consisting of complex microtubular arrays associated with a robust amorphous matrix that runs along the length of the cell. The microtubules support a subapical opening that facilitates phagocytosis of bacterial or eukaryotic prey cells. The structural complexity of the feeding apparatus varies among lineages; some taxa (i.e. petalomonads) feed with an apparatus composed of a simple pocket lined with a row of reinforcing microtubules (i.e. an MTR pocket), while other taxa feed using two or three robust rods and four internal folds, or "vanes" Leander et al., 2007, 2017; Lee & Simpson, 2014b; Triemer & Farmer, 1991a, 1991b).

The best synapomorphy for euglenids is the presence of a pellicle composed of a varying number of proteinaceous strips that can be longitudinally or helically arranged (Leander, 2004; Leander et al., 2007, 2017; Leander, Triemer, & Farmer, 2001; Leander, Witek, & Farmer, 2001). The number of strips that make up the pellicle is directly related to the plasticity of the cell, where lineages that contain fewer pellicle strips (<12) are rigid, and lineages that contain a large number of pellicle strips (>20) tend to be flexible and dynamic (Leander, 2004; Leander et al., 2007, 2017; Leander, Triemer, & Farmer, 2001; Leander, Witek, & Farmer, 2001). Plasticity, or the capability to undergo metaboly (e.g. euglenoid movement), in phagotrophic euglenids arose due to a series of permanent strip duplication events in a rigid ancestor, resulting in a multiplication of articulation zones between a larger number of narrower pellicle strips (Leander, 2004; Leander et al., 2007; Leander, Triemer, & Farmer, 2001). These strip duplication events resulted in a more dynamic pellicle associated with helically arranged strips in the most recent common ancestor of the monophyletic group Spirocuta (Cavalier-Smith, 2016; Lax et al., 2019; Leander, 2004; Leander et al., 2007; Leander, Witek, & Farmer, 2001; Lee & Simpson, 2014a; Paerschke et al., 2017).

Spirocuta is nested within a diverse array of rigid phagotrophic euglenids, such as the monophyletic petalomonads and a paraphyletic assemblage of phagotrophs with a robust feeding apparatus known as "ploeotids" (Lax et al., 2021, 2023). The feeding apparatus in ploeotids is always composed of two microtubular rods and four vanes; however, there is significant variation in the structural complexity of the feeding apparatus even among ploeotid taxa (Triemer & Farmer, 1991a, 1991b). Ploeotids also share a rigid pellicle composed of 10–12 longitudinally arranged pellicle strips and a distinctively thick ventral flagellum used for gliding (Lax et al., 2019; Leander, 2004; Leander et al., 2007, 2017). They represent much of the diversity of phagotrophic euglenids and consist of several distinct clades, as inferred from multigene phylogenetic analyses, including Alistosa and Karavia (Lax et al., 2021, 2023). The Spirocuta is a monophyletic group consisting of a paraphyletic assemblage of flexible phagotrophic lineages and two monophyletic subgroups: the osmotrophic Aphagea and the photosynthetic Euglenophyceae.

Olkasia is a monotypic genus of ploeotids represented by *O. polycarbonata*, which is known for its relatively large

cell size (~50 μm), distinct chisel-shaped feeding apparatus and 10 pronounced pellicle strips (Lax et al., 2019). The formal description of *Olkasia* arose as a result of a reclassification of a morphotype identified originally as *Ploeotia* c.f. *vitrea* (Lax & Simpson, 2013) due to morphological differences between *Ploeotia vitrea* and *Ploeotia* c.f. *vitrea* (= *O. polycarbonata*), and the consistent exclusion of *Ploeotia* c.f. *vitrea* from the *Ploeotia–Serpenomonas* clade in molecular phylogenetic analyses (Lax et al., 2019). In fact, molecular phylogenetic analyses of 18S rDNA sequences and multigene datasets place *O. polycarbonata* as the nearest sister lineage to the Spirocuta, forming the monophyletic group Olkaspira (Lax et al., 2019, 2021, 2023). This phylogenetic position makes *O. polycarbonata* a particularly important lineage for ultrastructural studies that aim to improve inferences about the evolution of traits in the most recent ancestors of Olkaspira and Spirocuta. Here, we report on the first ultrastructural data from *O. polycarbonata* using single-cell scanning and transmission electron microscopy (TEM), demonstrating several novel morphological traits associated with the feeding and flagellar apparatuses.

MATERIALS AND METHODS

Collection of organisms and light microscopy

Cells of *O. polycarbonata* were isolated from marine intertidal sediment collected within Akkeshi Bay, near Aininkappu Cape (43°00′23″N 144°51′22″E), Hokkaido, Japan, in June 2024. Sediment was transported to Akkeshi Marine Station for further processing. Cells of interest were concentrated into a Petri dish containing filtered seawater using a sea-ice extraction technique (Uhlig, 1964). Sea ice cubes (2–3) were placed on several tablespoons of sediment inside a PVC pipe wrapped in a 100 μm mesh filter. This extraction column containing marine sediment and sea ice was positioned directly on top of a Petri dish containing filtered seawater, and the ice was left to melt at room temperature overnight. Cells of interest passed through the 100 μm filter and were deposited into the Petri dish. The Petri dish was scanned for cells of *O. polycarbonata* using an Olympus CKX53 inverted microscope, which then were individually isolated using a hand-drawn, glass micropipette. Cells were placed on a coverslip for brightfield microscopy with an Olympus CKX53 inverted microscope and Kiss X8i DSLR camera (Canon, Tokyo, Japan). Several cells (Figures 1D,E and 6A) were mounted on a slide and photographed using an Olympus compound microscope and LabCam Ultra equipped with an iPhone 13 Mini.

Single-cell scanning electron microscopy (SEM)

Approximately eight to ten cells of *O. polycarbonata* were placed directly into a basket containing 2.5% glutaraldehyde (Electron Microscopy Sciences) buffered with 1.5X PHEM and 9% sucrose (Montanaro et al., 2016). Baskets were constructed using the blunt end of a trimmed pipette tip attached to an Isopore 10 μm membrane filter. Cells were kept in the PHEM glutaraldehyde solution at room temperature for 3–5 days before being washed in filtered seawater three times for 3 min each. Cells were postfixed using 1% osmium tetroxide (Electron Microscopy Sciences) (diluted in filtered seawater) for 10 min at room temperature and then washed three times in filtered seawater for 3 min per wash. Postfixed cells were washed with distilled water (three times for 3 min each) and then dehydrated using a graded ethanol series (30%, 50%, 70%, 85%, 90%, and 95%), incubating for 5 min at each step. Cells were further dehydrated in 100% EtOH for 5 min at room temperature, and then baskets containing dehydrated cells were dried in a critical point dryer using CO_2. Membranes were separated from the trimmed pipette tips upon removal from the critical point dryer, and membranes containing cells were mounted directly onto aluminum SEM stubs. Stubs containing the cells of interest were sputter coated with 2 nm of gold/palladium using a Cressington 208HR High Resolution Sputter Coater and viewed using a Zeiss XB350 Crossbeam SEM in the Bioimaging Facility at the University of British Columbia.

Single-cell transmission electron microscopy (TEM)

Approximately eight to ten cells of *O. polycarbonata* were placed directly into a basket containing 2.5% glutaraldehyde buffered with 1.5X PHEM and 9% sucrose (Montanaro et al., 2016) and fixed for 1 h at room temperature. Baskets were constructed using the blunt end of a trimmed pipette tip attached to the inner surface of a plastic Petri dish. Fixed cells were washed three times in filtered seawater for 3 min each and then were postfixed with 1% osmium tetroxide for 1 h and 30 min at room temperature. Postfixed cells were washed three times in filtered seawater and three times in distilled water for 3 min per wash. Cells were subsequently dehydrated using a graded ethanol series (30%, 50%, 70%, 85%, 90%, and 95%), incubating for 5 min at each step, and further dehydrated in 100% ethanol three times for 5 min each. Cells were then incubated in a 1:1 ratio of ethanol:acetone for 3 min, followed by a 10-min incubation step in 100% acetone at room temperature. Resin infiltration with Spurr's resin was performed by incubating the cells in a 1:1 ratio of acetone:resin (Spurr's Low Viscosity Embedding Kit, Electron Microscopy Sciences) for 1 h at room temperature, followed by two incubations in 100% resin for 10–12 h each. Infiltrated cells were then flat-embedded in a plastic Petri dish using 100% resin and placed into a drying oven set at 70°C for 36 h to polymerize. Flat-embedded cells were mounted

on an empty resin block at the appropriate orientation for sectioning. Ultra-thin serial sections were obtained from two cells using a Leica UC 6 Ultramicrotome and were mounted on Formvar-coated slot grids. Grids were imaged using a Tecnai Spirit TEM at the Bioimaging Facility at the University of British Columbia.

Light micrographs were adjusted for white balance and all micrographs of *O. polycarbonata* were processed and formatted into figure plates using Affinity Photo 2.

Whole-genome amplification and PCR

Approximately 10 individual cells of *O. polycarbonata* were isolated from sea-ice extractions, washed three times in filtered seawater, and collected individually into 0.2-μL microcentrifuge (PCR) tubes containing 9 μL of ultrapure RNase-free water (Invitrogen). Cells were kept frozen for ~2 weeks prior to amplification.

Isolated cells of *O. polycarbonata* were lysed using six to eight freeze–thaw cycles followed by incubation at 65°C for 3 min. Using the manufacturer's protocol, multiple displacement amplification (MDA) of DNA from each lysed cell was performed using an Illustra GenomiPhi V3 DNA amplification kit (GE Healthcare).

18S rDNA fragments from the MDA-amplified DNA were successfully amplified from three cells using a modified version of the PCR protocol outlined in Lax et al. (2019). PCR amplifications for each cell were carried out using PuReTaq Ready-To-Go PCR beads (Cytiva) with 22.5 μL of ultrapure RNase-free water (Invitrogen), 1.5 μL amplified DNA, and 0.5 μL of forward and reverse primers. We selected primers based on those reported by Lax et al. (2019) and

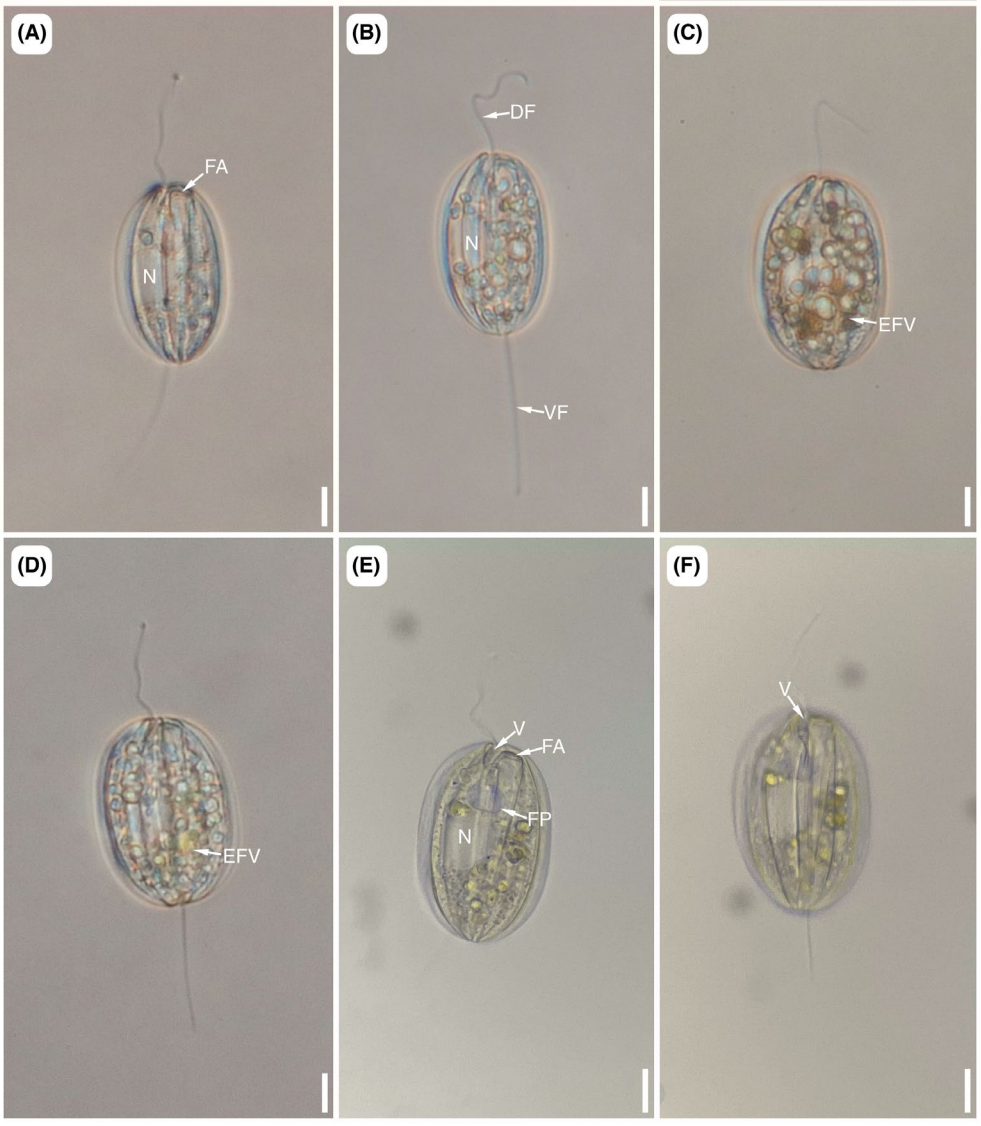

FIGURE 1 Light micrographs (LM) of five cells of *Olkasia polycarbonata*. (A–D) Micrographs showing the nucleus (N), capped feeding apparatus (FA), dorsal flagellum (DF), and ventral flagellum (VF). Some cells (C and D) contain large, digested food vacuoles (EFV). (E and F). LMs showing the vestibulum (V) of one cell at two planes of focus. Flagella are inserted into the flagellar pocket (FP). Scale bars = 10 μm.

performed two PCR amplifications to sequence the entire 18S rRNA gene of the *O. polycarbonata* isolates. The first primer set consisted of forward primer EukA (AACCTGGTTGATCCTGCCAGT) and reverse primer EzoaR (GGRGCATCACAGACCTGC). The second primer set consisted of the forward primer Ploeo2F (AAATTACCCAATGSCAAC) and reverse primer EukB (TGATCCTTCTGCAGGTTCACCTAC). PCR incubation conditions were identical to those outlined in Lax et al. (2019), except for the annealing temperature, which was 52°C for both reactions. To check if the 18S rDNA sequences were correctly amplified, 5 μL of each PCR product was loaded onto a 1% agarose gel stained with GelRed™ (Biotium). PCR products were purified using ExoSAPIT™ (Applied Biosystems) and Sanger DNA sequencing was carried out by Genewiz (Azenta Life Sciences).

Molecular phylogenetic analyses

We manually checked the 18S rDNA sequences for ambiguities and assembled them into contigs using Geneious Prime 2024.0.4. Primer sequences were trimmed from the 5′ and 3′ ends of each sequence prior to assembly. The resulting assembled sequences demonstrated high similarity with *O. polycarbonata* sequences from Lax et al. (2019) based on a BLAST analysis, particularly with cells from *Olkasia polycarbonata* Clade A (KS3, KS1, U4, and UB41). DNA sequence identities ranged from 97.1% to 98.9%. We completed a pairwise alignment between sequences obtained in this study and existing *Olkasia* sequences with lengths >1000 bp. Percent identity (obtained from BLAST) and pairwise identity scores of all 18S rDNA sequences obtained in this study and previously reported *O. polycarbonata* sequences can be found in Table S1. Sequences were deposited to GenBank and accession numbers are as follows: No. PQ622968, No. PQ622966, and No. PQ622967 for isolates OLK1, OLK3, and OLK7, respectively.

The DNA sequences obtained in this study were aligned against a modified alignment from Lax et al. (2019) using the MAFFT v7.511 FFT-NS-i web server (Katoh et al., 2019). *Chelandium granulatum* BB14, *Gaulosia striata* BB9, and *Decastava* sp. SPO2 were also included (Lax et al., 2023). The 1445 bp alignment (18S_Ploeotids_MAFFT_untrimmed) contained 118 taxa and was masked using the Geneious Prime algorithm to remove nonconserved regions by removing ambiguously aligned sites and all sites containing at least 10% gaps. Alignments were checked for ambiguously aligned sites and adjusted by eye using AliView v1.28 (Larsson, 2014). Long-branching taxa, short sequences (<1000 bp), and taxa identified as rogues in Lax et al. (2019) were excluded from this alignment to reduce artifacts.

According to a model test performed using IQTREE 2.3.6 (Minh et al., 2020), the best-fitting model for nucleotide evolution for this alignment was GTR+F+I+G4, based on the Bayesian information criterion (BIC) score. We inferred a maximum-likelihood tree under the GTR+F+I+G4 model using RAxML-GUI version 2.0.10 (Edler et al., 2020) with a nonparametric bootstrap analysis of 1000 bootstrap replicates.

RESULTS

General morphology

Live cells of *O. polycarbonata* were dorsoventrally flattened, 46–52 μm long by 30–33 μm wide (n=7), and colorless, except for large food vacuoles present in the cytoplasm at the middle and posterior end of the cell (Figures 1, 2, 3B). The flagella were heterodynamic and inserted subapically into the flagellar pocket through the vestibulum, which was positioned to the left of the feeding apparatus (Figure 1E). The ventral flagellum was consistently longer than the dorsal flagellum, at 1.5X–1.8X the cell length, and appeared thickened relative to the dorsal flagellum. The dorsal flagellum was 0.7X–0.8X the cell length. Live cells were rigid, and gliding movement was typical of ploeotids. The nucleus was large and positioned on the left side of the cell about halfway down the length of the cell, immediately after the base of the flagellar pocket. The general morphology and behavior of *O. polycarbonata* were consistent with the original description of this species by Lax et al. (2019).

Cell surface and pellicle structure

Cells of *O. polycarbonata* possessed 10 longitudinally arranged pellicle strips that were each about 8 μm wide. The lateral margins of each broad strip were raised at the articulation zones between strips, forming 10 distinct ridges (Figures 2 and 3A,C). A uniform row of microtubules subtended each pellicle strip, followed by cisternae of rough endoplasmic reticulum (Figure 3A–C). The arch of each strip was concave and was conspicuously thickened and tapered toward the articulation zones. Pore-like openings in the middle of a pellicle strip, and not near the articulation zones, were sometimes present (Figure 3B). No other pores were observed by TEM or SEM. The surface of the pellicle strips in *O. polycarbonata* was generally smooth except for slight texturing observed at high magnifications with SEM (Figure 2E). Discharged extrusomes were observed on the cell surface and appeared to originate from the articulation zones between two strips (Figure 2A).

Rod-shaped bacteria were observed on the surface of several cells of *O. polycarbonata*, though in low abundance (Figures 2E and 3A,B). The bacteria were 0.8–1.2 μm long by 0.4 μm wide and were attached perpendicular to the cell surface. Several bacteria were

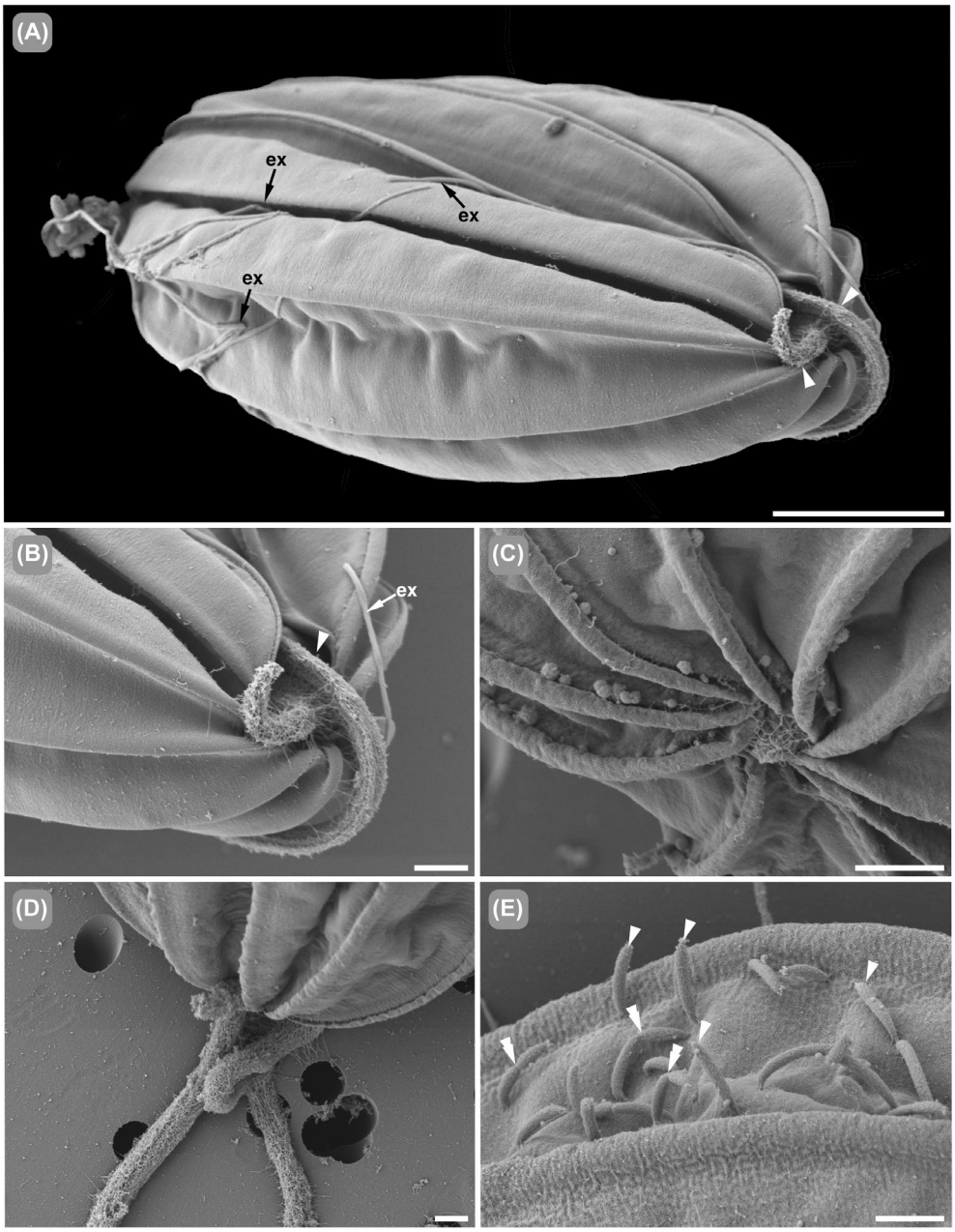

FIGURE 2 Scanning electron micrographs (SEMs) of *Olkasia polycarbonata*. (A) Low-magnification SEM showing two flagella (arrowheads) emerging from the vestibulum and tubular extrusomes (ex) ejected from beneath the cell surface. Scale bar = 10 μm. (B) High-magnification ventral view of the anterior end of the cell showing the flagella emerging from the vestibular opening (arrowhead) and tubular extrusomes (ex). (C) High-magnification SEM of the posterior end of the cell showing 10 pellicle strip junctions. (D) Dorsal view of the anterior end of the cell showing two flagella covered in flagellar hairs (mastigonemes). (E) High-magnification SEM of a pellicle strip articulation zone showing cell surface bacteria (arrowheads), some of which are dividing (double arrowheads). Scale bars B–E = 2 μm.

observed dividing by binary fission on the cell surface (double arrowheads; Figure 2E).

Cytoplasmic organelles

The cytoplasm of *O. polycarbonata* contained a large nucleus (~10 μm in diameter) with permanently condensed chromosomes and a robust nucleolus (Figures 1 and 3D). Neither the condensed chromatin nor the nucleolus was observed with light microscopy. Mitochondria with discoidal cristae and large Golgi bodies with densely packed cisternae were distributed throughout the cytoplasm of the cell (Figure 4A,B). Several food vacuoles with partially digested contents were observed with both light microscopy and TEM at the middle and posterior regions of the cell (Figures 1C and 3A). The material undergoing digestion within these food vacuoles was large (2.7–4.2 μm in diameter), indicating that the contents are likely remnants of eukaryotic prey cells.

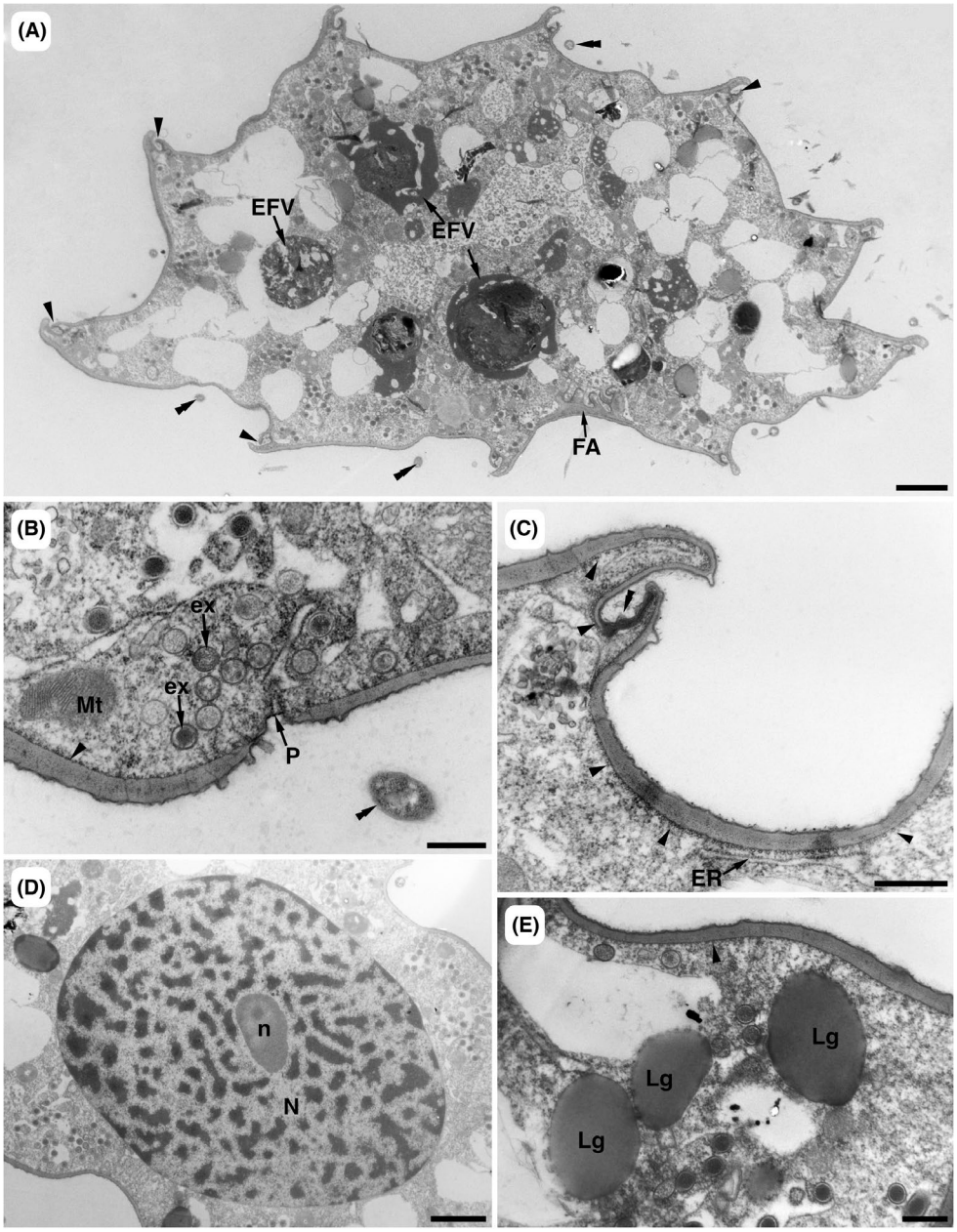

FIGURE 3 Transmission electron micrographs (TEMs) of *Olkasia polycarbonata* in cross-section. (A) Low-magnification TEM showing the articulation zones between pellicle strips (arrowheads), cell surface bacteria (double arrowheads), and eukaryotic food vacuoles (EFV). Scale bar = 2 μm. (B) High-magnification TEM of the cell surface showing a mitochondrion (Mt), tubular extrusomes (ex), microtubules underlying the pellicle strips (arrowheads), bacteria (double arrowheads), and a pore (arrow) through a pellicle strip. Scale bar = 0.5 μm. (C) High-magnification TEM of the articulation zone (double arrowhead) between pellicle strips showing underlying microtubules (arrowheads) and cisternae of rough endoplasmic reticulum (ER). Scale bar = 0.5 μm. (D) Low-magnification TEM of the nucleus (N) and nucleolus (n). Scale bar = 2 μm. (E) High-magnification TEM showing lipid globules (Lg) present in the cytoplasm. Scale bar = 0.5 μm.

Tubular extrusomes were 200 nm in diameter and present either individually or in small clusters throughout the entire cytoplasm; however, the extrusomes were more frequently observed at the periphery of the cell, especially near the articulation zones between pellicle strips (Figures 3A,B and 4C,D). Regularly repeating structures that resembled extrusomal docking sites were observed in the articulation zone between two pellicle strips, and undischarged extrusomes were oriented longitudinally, underlying the cisternae of rough endoplasmic reticulum beneath each strip (Figures 4E and 5A). Tubular extrusomes consisted of a thick outer wall with helical striations (arrowhead, Figure 4D) and an electron-dense inner core arranged in a honeycomb-like matrix (double arrowhead, Figure 4D). Transverse sections through different positions along the length of the

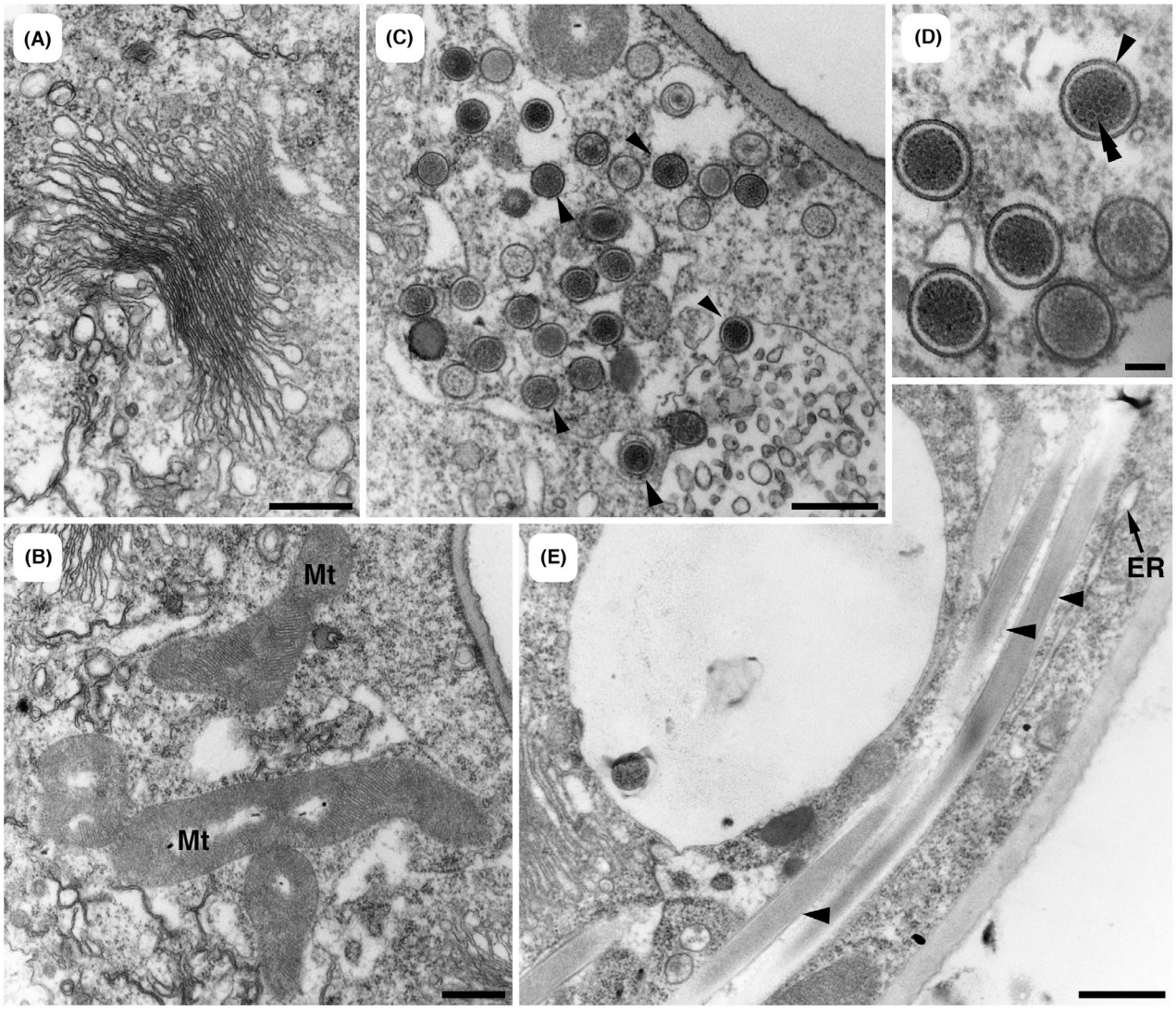

FIGURE 4 Transmission electron micrographs (TEMs) of the Golgi apparatus, mitochondria, and tubular extrusomes of *Olkasia polycarbonata*. (A) High-magnification TEM of a tightly packed Golgi body. (B) High-magnification TEM of several mitochondria (Mt) with discoidal cristae. (C) Cross-sectional TEM through a cluster of tubular extrusomes (arrowheads). Scale bars A–C = 0.5 μm. (D) High-magnification TEM of several tubular extrusomes showing a ribbed exterior (arrowhead) and a distinct honeycomb matrix inside of each extrusome (double arrowhead). Scale bar = 100 nm. (E) Longitudinal TEM showing several tubular extrusomes (arrowheads) present near the periphery of the cell and cisternae of endoplasmic reticulum (ER) situated between the extrusomes and the cell surface. Scale bar = 0.5 μm.

tubular extrusomes showed variations in internal organization, suggesting that these organelles have a complex three-dimensional ultrastructure (Figures 3B and 4C,D).

Vestibulum and feeding apparatus

The vestibular opening of *O. polycarbonata* developed as an invagination at the apical end of the cell and formed the opening to the feeding pocket and the flagellar pocket (Figure 5A–C). Fine hairs, or a tomentum, were observed near the vestibular opening at the anterior end of the cell (Figure 5C). The dorsal face of the vestibulum was lined by a singular row of microtubules followed by an amorphous matrix that housed the dorsal and ventral feeding rods (Figure 5B). The lateral side of the dorsal face of the flagellar pocket at the level of the vestibulum was lined by 10 supportive strips (Figure 5B,C). On the medial side of the flagellar pocket, lateral to the ventral rod of the feeding apparatus and at the level of the vestibulum, there was a hook-like structure that resembled the base of a putative feeding comb (Figure 5B). An electron-dense structure lined the medial side of the ventral rod of the feeding apparatus (Figure 5B).

The feeding apparatus of *O. polycarbonata* extended almost down the entire length of the cell and contained two microtubular rods and four folded vanes (Figures 1, 5B, 6). The vanes of the feeding apparatus maintained their organization throughout its length. At the level of the vestibulum, the dorsal rod was composed of 26 rows

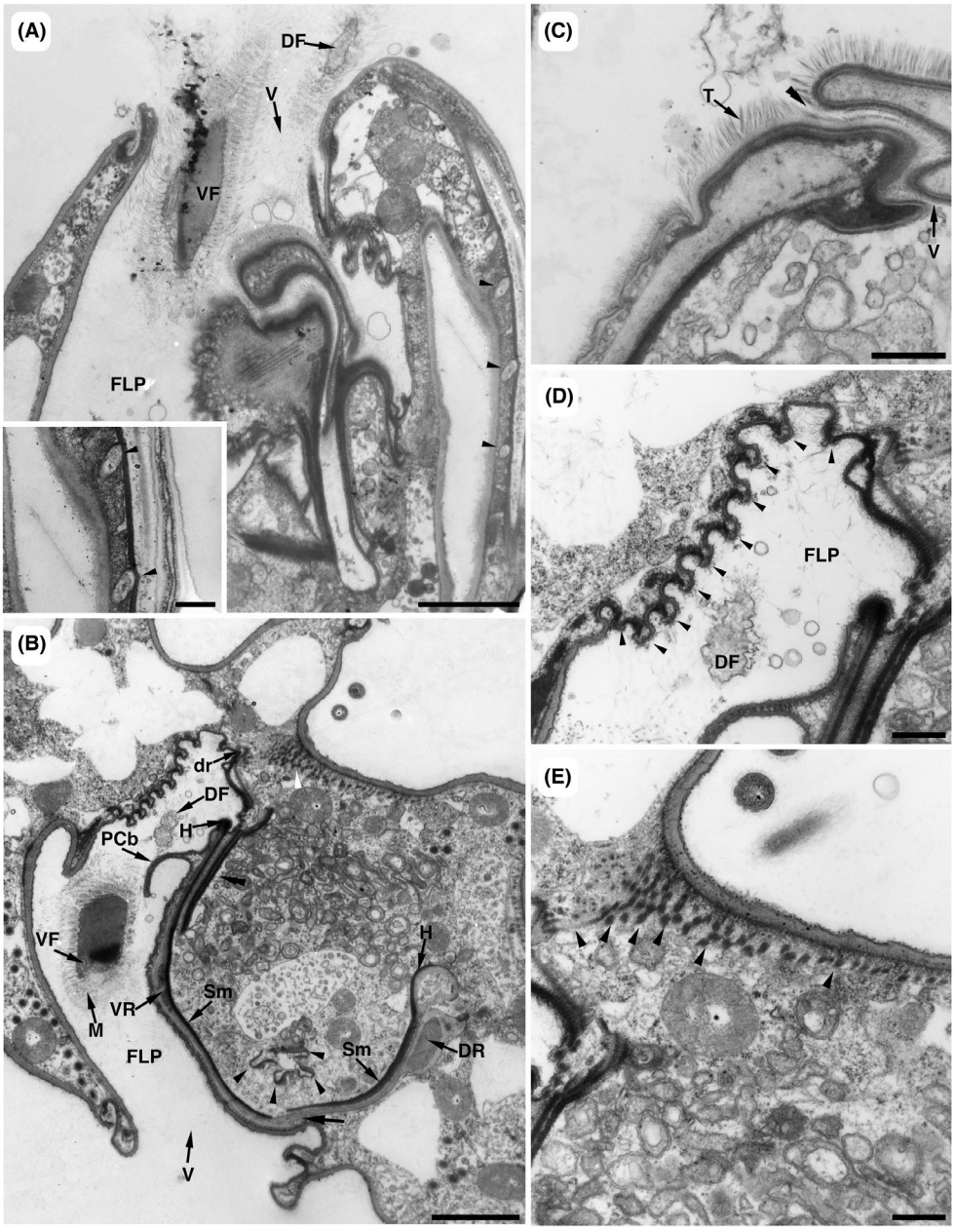

FIGURE 5 Transmission electron micrographs (TEMs) of the vestibulum of *Olkasia polycarbonata*. (A) Longitudinal TEM through the anterior region of a cell showing the flagellar pocket (FLP), ventral flagellum (VF), dorsal flagellum (DF), extrusome docking sites (arrowheads), and the vestibular opening (V). Scale bar = 2 μm. Inset. High-magnification view of two extrusome docking sites. Scale bar 0.5 μm. (B) Cross-section through the vestibulum showing the ventral rod (VR) and dorsal rod (DR) of the feeding apparatus. Four plicate vanes (arrowheads) are positioned between both rods and two sets of supportive microtubules (Sm) run adjacent to both rods that form hook-like structures (H). Double arrowheads show an electron-dense microtubular structure on the medial side of the ventral rod. PCb = putative feeding comb. Dorsal root (dr) microtubules reinforce the dorsal side of the flagellar pocket and are associated with the electron-dense threads (white arrowheads). Mastigonemes (M) are associated with the ventral flagellum (VF). Scale bar = 2 μm. (C) Longitudinal TEM showing a gap in the pellicle (double arrowhead) and the tomentum (T), both associated with the vestibular opening (V). (D) Ten strips (arrowheads) line the inside of the vestibulum reinforcing the flagellar pocket. (E) High-magnification TEM of electron-dense threads situated beneath a dorsal pellicle strip. Scale bars C–E = 0.5 μm.

of microtubules that formed a large bundle, while the ventral rod was composed of two smaller bundles of microtubules (Figure 5B). Both rods were surrounded by an amorphous matrix that extended medially toward one another and became contiguous near the feeding vanes, separated by a thin membrane (arrow; Figure 5B). This membrane was not observed posterior to the level shown in Figure 5B (Figure 6B).

At the anterior end of the feeding apparatus, but posterior to the region shown in Figure 5B, the rods formed a conspicuous "V" shape around the four vanes, which were arranged like a pinwheel (Figure 6C). Both feeding

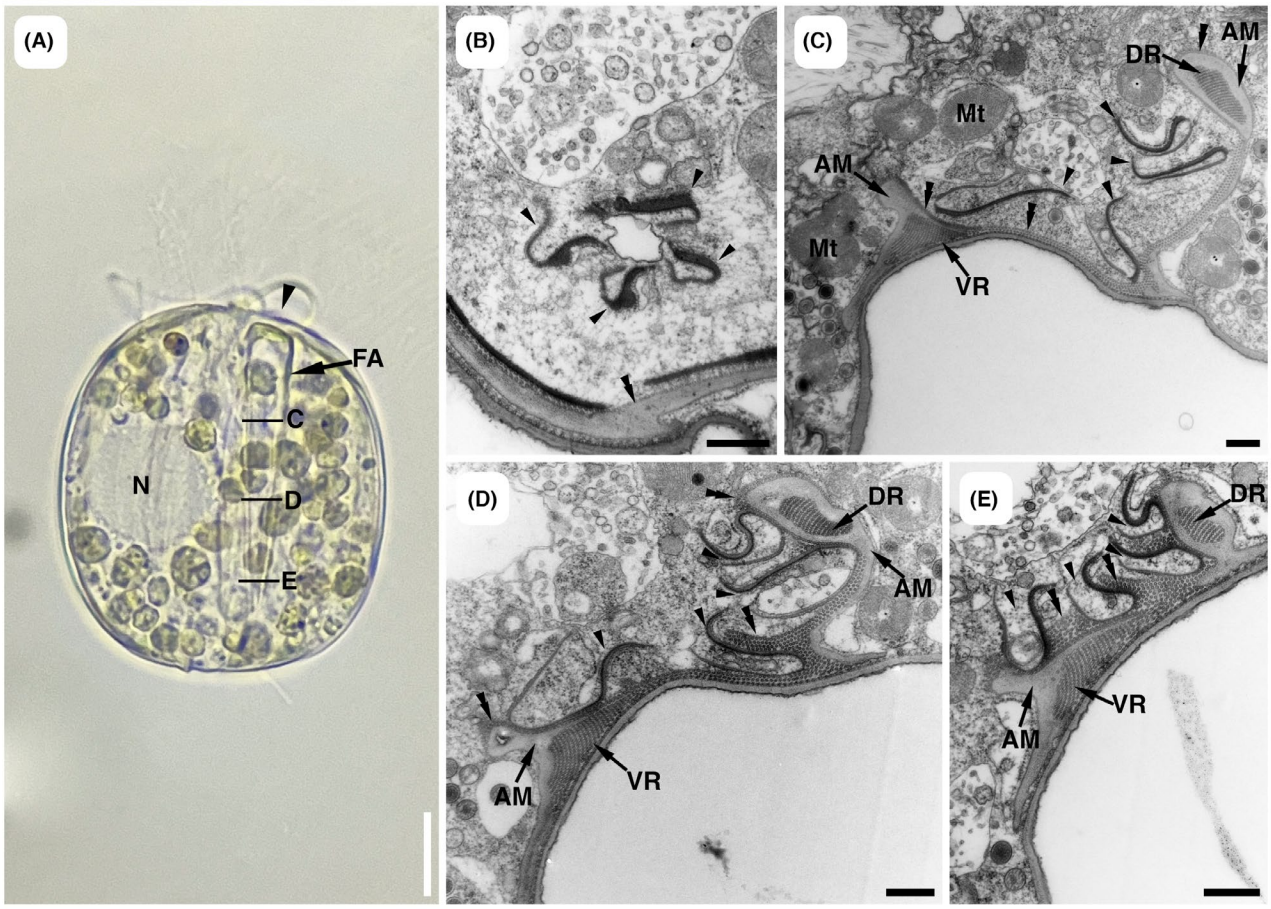

FIGURE 6 Transmission electron micrographs (TEMs) showing the feeding apparatus of *Olkasia polycarbonata* from the anterior to posterior region of the cell. (A) Light micrograph (LM) of a cell squished under a coverslip to clearly show the nucleus (N) and feeding apparatus (FA). The approximate regions of the feeding apparatus shown in Figures C–E are labeled accordingly. Scale bar = 10 μm. (B) TEM of the anterior region of four vanes associated with the feeding apparatus (arrowheads). (C–E) Cross-sectional TEMs of the feeding apparatus, pictured from anterior (C) to posterior (E) ends, showing the ventral rod (VR), dorsal rod (DR), and four vanes (arrowheads). Amorphous matrix surrounding each feeding rod is shown (AM). (C) Anterior region of the feeding apparatus where the vanes are not yet connected to the DR or the VR. Supportive microtubules (double arrowheads) line the outside of the dorsal and ventral faces of the amorphous matrix surrounding the ventral rod. These microtubules extend toward and line the outside of the amorphous matrix surrounding the dorsal rod. (D) Cross-sectional TEM through the middle of the feeding apparatus showing four vanes associated with the supportive microtubules of both feeding rods (VR and DR). More supportive microtubules (double arrowheads) are present between the ventral and dorsal rods of the feeding apparatus, surrounding and connecting both feeding rods. (E) Cross-sectional TEM through the posterior end of the feeding apparatus shows bundles of supportive microtubules between each vane (double arrowheads). Scale bars B–E = 0.5 μm.

rods were well developed, consisting of distinct microtubular arrays that were maintained down the length of the entire feeding apparatus (Figure 6C–E). The amorphous matrix surrounding the ventral rod no longer extended toward the dorsal rod and was only maintained adjacent to the dorsal face of the ventral rod. The amorphous matrix surrounding the dorsal rod extended ventrally toward the pellicle (Figure 6C–E).

A row of microtubules, henceforth referred to as "supportive microtubules" for the remainder of this paper, ran adjacent to the amorphous matrices of each feeding rod and extended dorsally past each rod, forming two hook-like structures at the anterior end of the cell that reinforced the feeding apparatus (Figure 5B). These supportive microtubules originated at the base of the feeding apparatus and extended longitudinally along the amorphous matrix of each rod, parallel to the internal microtubules that formed both feeding rods (double arrowheads; Figure 6B–E). At the anterior end of the feeding apparatus, the microtubules that formed the ventral rod were not continuous with the supportive microtubules; however, they became continuous from the midpoint to the posterior end of the feeding apparatus (Figure 6D,E). The amorphous matrix continuously surrounded the microtubules that formed the dorsal rod, which never became continuous with the surrounding supportive microtubules (double arrowheads; Figure 6C–E).

The four vanes of the feeding apparatus did not interact directly with the microtubular arrays that formed both feeding rods. Instead, these vanes became continuous with the supportive microtubules lining

the dorsal side of the feeding apparatus about midway down the cell (Figure 6D). This supportive microtubular structure that surrounded the amorphous matrix of each rod became more developed toward the posterior end of the feeding apparatus, starting from a few rows of microtubules at the anterior end to prominent microtubular arrays positioned between each vane at the base (Figure 6B–E).

Flagella, flagellar transition zone, and flagellar root system

The flagella of *O. polycarbonata* are inserted at the base of the flagellar pocket, positioned directly anterior to the nucleus, and extended through the flagellar pocket, emerging from the vestibular opening at the anterior end of the cell. Each flagellum consisted of a 9+2 microtubular axoneme and a paraxonemal rod (Figures 5 and 7). Fine flagellar hairs (mastigonemes) were observed primarily in association with the ventral flagellum at the anterior end of the flagellar pocket near the vestibular opening (Figures 5B and 7B). The dorsal flagellum, which was narrower than the ventral flagellum, contained a whorled microtubular paraxonemal rod that became thicker toward the base of the flagellar pocket (0.4 μm in diameter in Figure 5D to 0.8 μm in diameter in Figure 7E). In contrast, the ventral flagellum was up to 2.4 μm wide at its thickest point and contained a lattice-like paraxonemal rod (Figure 7). The ventral paraxonemal rod drastically changed in shape and structure toward the base of the flagellar pocket when viewed from the anterior end of the cell (Figure 7C–E). At the distal end of the ventral flagellum, the paraxonemal rod was rectangular in shape. It contained a long electron-dense inclusion positioned adjacent to the 9+2 microtubular axoneme and ran nearly the entire width of the paraxonemal rod (Figure 7C). Near the middle of the flagellar pocket, distal to the flagellar transition zone, the ventral paraxonemal rod appeared elongated, and the electron-dense inclusion became significantly smaller (Figure 7D). A prominent fibrous swelling was present on both flagella adjacent to the paraxonemal rods (Figure 7D). Although these swellings were relatively large compared to the overall size of each flagellum, they did not extend far longitudinally in either direction.

The microtubular axonemes for both flagella lost their central microtubules just before the base of the flagellar pocket, resulting in the 9+0 microtubular organization that indicated the flagellar transition zone (Figure 7E). The ventral paraxonemal rod had elongated into a V-shape, and the flagellar swellings observed in Figure 7D were no longer present. The flagella were inserted into the base of the flagellar pocket. Two basal bodies (the dorsal and ventral basal bodies) and three microtubular roots (the ventral, dorsal, and intermediate roots, or R2, R3, and R1, respectively) formed the flagellar apparatus (Figure 7F). Two smaller accessory basal bodies were present: the dorsal and ventral accessory basal bodies.

The dorsal and ventral roots lined the entire length of the flagellar pocket and provided structural support (Figure 7A,C–E). The microtubules that formed the dorsal root were continuous with the microtubules that subtend the minor groove of a dorsal pellicle strip via electron-dense threads (Figure 5E). The intermediate root was lateral to the ventral flagellum near the middle of the flagellar pocket (Figure 7D). The intermediate root was connected to the dorsal basal body, situated between both basal bodies, and associated with a striated connective fiber (Figure 7F). The dorsal and ventral flagellar roots originated from their respective basal body, and a ventral lamina supported the ventral root.

Molecular phylogenetic analyses

To confirm the identity of *O. polycarbonata*, 18S rDNA sequences from three individually isolated cells collected at the same time and from the same sample as the individual cells isolated for electron microscopy were sequenced. We obtained a nearly full-length sequence for one isolate, OLK 3 (1944 bp), and truncated sequences from two isolates: OLK 7 and OLK 1 (1663 and 1215 bp, respectively). Pairwise identities of *O. polycarbonata* sequences obtained in this study ranged from 98.5% to 99.1%. The sequence similarities between the sequences obtained in this study and *O. polycarbonata* sequences previously deposited on NCBI ranged from 94.5% to 98.6% for Clade A and 87.3% to 93.9% for Clade B based on a pairwise alignment (Table S1).

A maximum-likelihood molecular phylogenetic analysis was performed using the 118-taxon alignment and demonstrated that the isolates of *O. polycarbonata* obtained in this study form a monophyletic group with the other *O. polycarbonata* isolates reported in Lax et al. (2019) with 100% bootstrap support (Figure 8). *Chelandium granulatum* branched sister to the *O. polycarbonata* clade, albeit with only modest statistical support (80%), and formed a clade that is sister to the Spirocuta (Figure 8).

DISCUSSION

The ultrastructural data from *O. polycarbonata* demonstrated several similarities with other ploeotids, namely (1) a rigid pellicle consisting of 10 longitudinally arranged pellicle strips, (2) a thin dorsal flagellum and a thicker ventral flagellum associated with gliding, and (3) a feeding apparatus composed of two robust microtubular rods and four vanes organized as a central pinwheel. However, the ultrastructure data reported here also demonstrated several cytoskeletal traits in

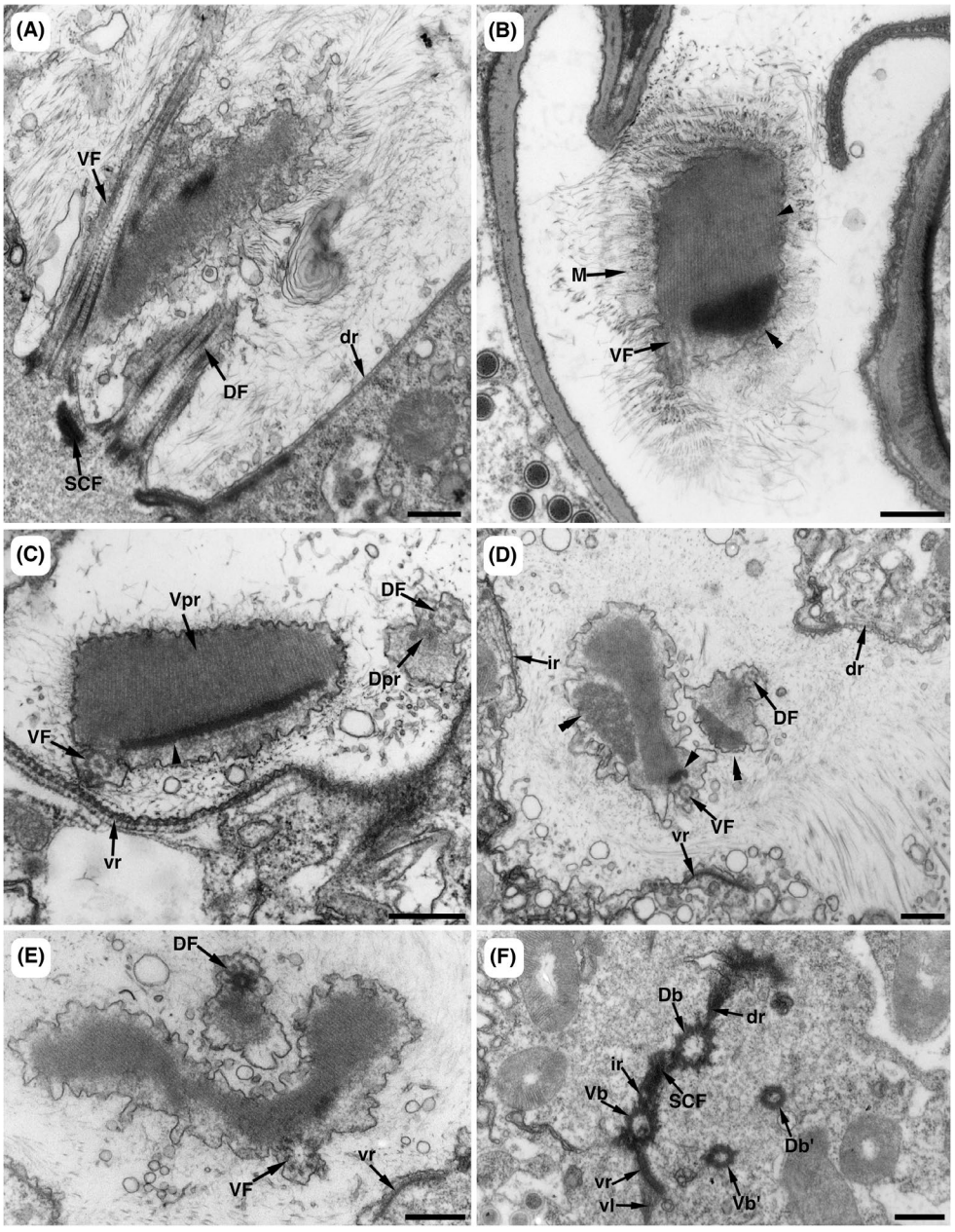

FIGURE 7 Transmission electron micrographs (TEM) of the flagellar root system of *O. polycarbonata*. (A) Longitudinal TEM of the base of the flagellar pocket showing the ventral flagellum (VF), dorsal flagellum (DF), and dorsal microtubular root (dr). A striated connecting fiber (SCF) can be seen between the microtubular roots (arrowheads) of both flagella. (B–E) Cross-sections through the flagellar pocket showing the flagella, pictured from the distal (B) to proximal (E) ends of the flagellar pocket. (B) TEM of the ventral flagellum (VF) at the distal end of the flagellar pocket showing a lattice-like paraxonemal rod (arrowhead) associated with an electron-dense fibrous structure (double arrowhead). Mastigonemes surround the ventral flagellum (M). (C) Section through the dorsal and ventral flagella (DF; VF) showing a 9+2 microtubular axoneme and paraxonemal rod present in both flagella. The distal end of the ventral flagellar root (vr) is shown. The ventral paraxonemal rod (Vpr) is continuously associated with an electron-dense fibrous structure (arrowhead). The paraxonemal rods of each flagellum differ in size and structure, where the ventral paraxonemal rod (Vpr) is larger and lattice like in organization in contrast to the dorsal paraxonemal rod (Dpr), which is smaller and tubular in structure. (D) TEM of the flagella at the middle of the flagellar pocket showing the ventral root (vr), intermediate root (ir), and dorsal root (dr) of the flagellar apparatus. A fibrous structure is associated with the paraxonemal rod of each flagellum (double arrowheads). (E) Section through the flagellar pocket near the point of insertion showing the flagellar transition zone. Due to the loss of central axonemal microtubules, the dorsal and ventral flagellar axonemes exhibit a 9+0 microtubular organization. (F) Section showing the flagellar basal bodies (Db; Vb), flagellar root system, and accessory basal bodies (Db′; Vb'). The ventral root (vr) and vr-associated ventral lamina (vl) extend from the ventral basal body (Vb); the dorsal root (dr) extends from the dorsal basal body (Db). The intermediate root (ir) and a striated connecting fiber link the two basal bodies. All scale bars = 0.5 μm.

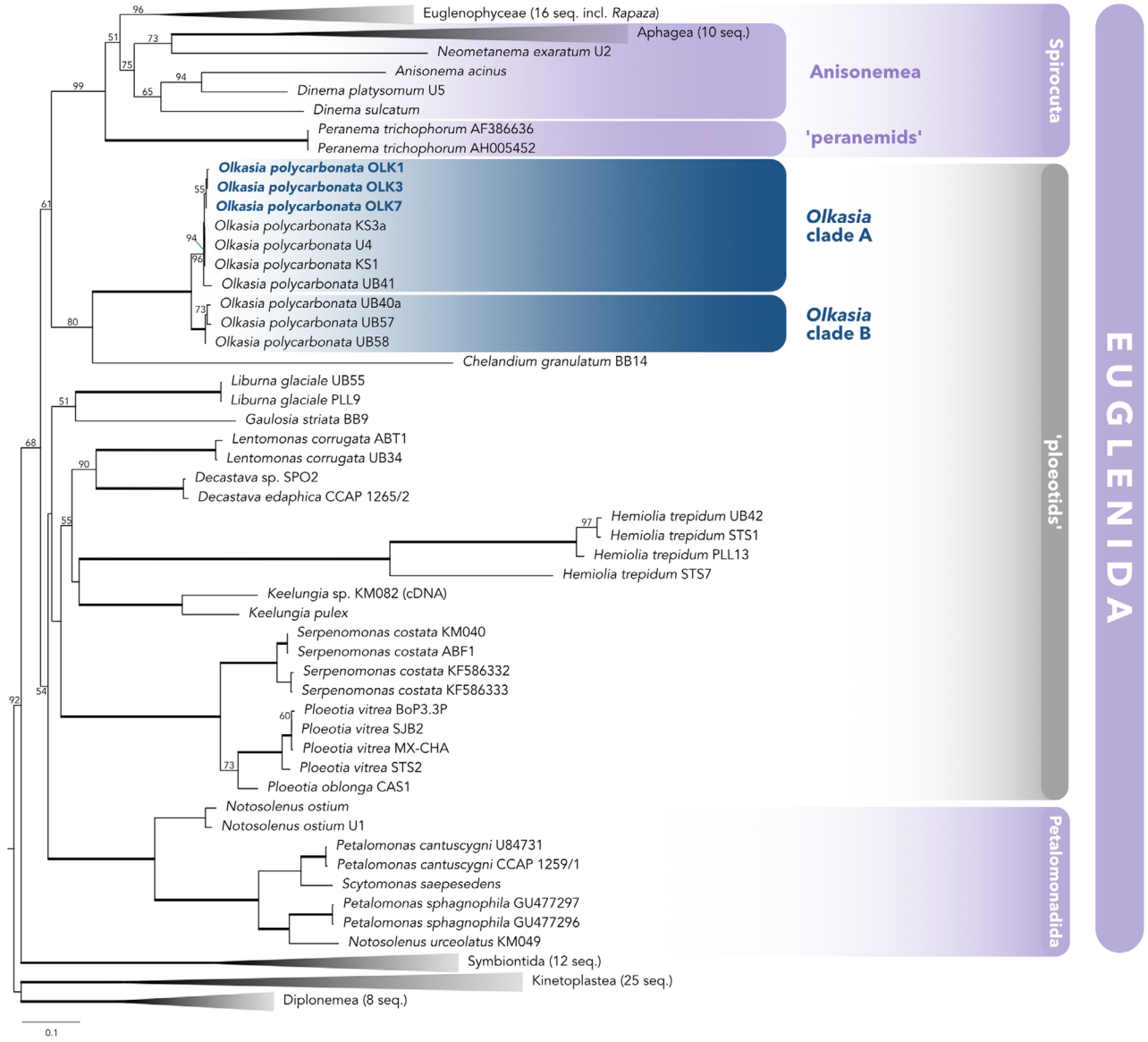

FIGURE 8 Maximum-likelihood phylogeny inferred from 18S rDNA sequences showing the position of *O. polycarbonata* under the GTR+F+I+G4 model. *O. polycarbonata* sequences from this study are in bold. Major groups of euglenids are indicated and the tree is rooted using kinetoplastids and diplonemids as an outgroup. Thickened branches indicate 100% bootstrap support. Support values below 50% are not shown.

O. polycarbonata that are either novel or have been previously reported but are not well characterized.

Pellicle architecture

The pellicle of *O. polycarbonata* consists of 10 longitudinally arranged proteinaceous pellicle strips that are elevated along the margins and form ridges at the articulation zones, similar to the pellicle strips of several other ploeotids, such as *Serpenomonas costata* and *Lentomonas corrugata* (Farmer & Triemer, 1994; Linton & Triemer, 1999). Each pellicle strip in *O. polycarbonata* was thicker than the strips reported in other ploeotids and other members of Olkaspira (Leander & Farmer, 2001). Dense accumulations of tubular extrusomes with a distinct honeycomb-like internal architecture were present beneath the pellicle. This honeycomb-like architecture is dissimilar from the cross-like architecture observed in the tubular extrusomes of some euglenozoans and, so far as we know, has never before been reported in the tubular extrusomes found in euglenids (Leander et al., 2017).

A pore in the middle of a pellicle strip, rather than within the articulation zones between strips, has not been previously reported in euglenids. This pore could function either as an extrusomal docking site or for vesicular transport. Moreover, the presence of bacteria on the cell surface of *O. polycarbonta* was not previously reported by Lax et al. (2019). Epibiotic bacteria have

been documented in several different euglenid lineages so far, namely *Dylakosoma pelophilum* (Wolowski, 1995), *Euglena helicoideus* (Leander & Farmer, 2000a, 2000b), and *Ploeotia vitrea* (Patterson & Simpson, 1996). The epibionts of *D. pelophilum* and *E. helicoideus* do not bear ultrastructural similarity in organization on the cell surface with the bacteria associated with the cell surface in *O. polycarbonata*. However, the sparse distribution of bacteria observed on the cell surface of *Ploeotia vitrea* in Patterson and Simpson (1996) is comparable to the organization and distribution of the bacteria we observed in *O. polycarbonata*.

The presence of partially digested eukaryotic prey in the cytoplasm of *O. polycarbonata* is consistent with the eukaryotic food vacuoles reported by Lax et al. (2019) and further demonstrates that euglenids with a rigid pellicle are not limited to bacterivory. Other rigid euglenids, such as *Dolium sedentarium* (a petalomonad) and karavid ploeotids (e.g. *Liburna* and *Hemiolia*), have been observed to contain whole ingested pennate diatoms within the cytoplasm, indicating that they are capable of whole-cell phagocytosis of diatoms despite possessing a rigid pellicle (Al-Qassab et al., 2002; Lax et al., 2019, 2023). As ultrastructural information on *D. sedentarium* and members of the Karavia is absent from the literature, further investigation into either of these two groups may demonstrate additional cytoskeletal traits that are involved in the consumption of large eukaryotic prey in the absence of a flexible pellicle.

Feeding apparatus

Triemer and Farmer (1991a, 1991b) proposed four distinct types of feeding apparatuses in euglenids based on differences in the overall organization of microtubules lining the pocket, rods, and vanes across eight taxa. Types I and II are associated with rigid bacterivorous euglenids like petalomonads and *Serpenomonas costata*, although the latter species can also consume yeast cells (Breglia et al., 2013; Linton & Triemer, 1999). A Type I feeding apparatus is found in petalomonads and consists of a simple pocket reinforced by a lining of microtubules (syn., MTR pocket) (Linton & Triemer, 1999). A Type II feeding apparatus is found in *S. costata* and consists of two rods composed of an amorphous matrix and four plicate vanes (Triemer & Farmer, 1991a). Type III feeding apparatuses also consist of two rods and four vanes; however, they are more complex, primarily found in flexible phagotrophic euglenids (e.g. *Dinema*, *Peranema*, and *Teloprocta*) and contain well-developed microtubular structures, such as accessory rods and lamellae, that reinforce the rods and vanes (Breglia et al., 2013; Nisbet, 1974; Triemer & Farmer, 1991a). Several rigid euglenids also possess a feeding apparatus that conforms to Type III, such as *Lentomonas corrugata* and *Keelungia pulex*, but these are less robust than those observed in phagotrophic members of the Spirocuta (Chan et al., 2013; Farmer & Triemer, 1994). The fourth type of feeding apparatus (Type IV) has only been observed in *Entosiphon* thus far and is distinguished from the other feeding apparatus types by the presence of an additional microtubular rod forming a "C"-shaped siphon. This siphon is in constant motion, extending forward within the vestibulum during feeding (Triemer & Farmer, 1991a, 1991b; Triemer & Fritz, 1987).

The feeding apparatus of *O. polycarbonata* most closely resembles a Type III feeding apparatus according to Triemer and Farmer's system. The feeding rods of *O. polycarbonata* each contained over 200 microtubules, which is more similar to the numbers observed in flexible phagotrophic euglenids (e.g. *Peranema trichophorum* and *Telonema scaphurum*) than to the ploeotid species studied so far (e.g. *S. costata*, *Lentomonas corrugata*, and *Keelungia pulex*), which have less than 20 microtubules per rod (Breglia et al., 2013; Chan et al., 2013; Farmer & Triemer, 1994; Nisbet, 1974). The overall organization of the feeding apparatus of *O. polycarbonata* is similar to the feeding apparatus of *Lentomonas corrugata* (= *L. applanatum*), which was inferred to represent an intermediate state between ploeotids and spirocutes like *Urceolus* (Farmer & Triemer, 1994). The electron-dense microtubular structure we observed in *O. polycarbonata* (double arrowheads; Figure 5B) has also been observed in *L. corrugata*, although the function of this structure remains unknown. Moreover, the supportive microtubules that reinforce the base of the vanes in *O. polycarbonata* and run longitudinally along the outside of each feeding rod are also present in several other ploeotids, such as *L. corrugata* and *S. costata*. However, the structures formed from these supportive microtubules in *L. corrugata* and *S. costata* are noticeably smaller and less complex compared to those in *O. polycarbonata*.

Supportive microtubules that reinforce the rods and vanes of the feeding apparatus in *O. polycarbonata* are also present in *Peranema trichophorum* and *Urceolus cyclostomus* (Nisbet, 1974; Triemer & Farmer, 1991a). The phylogenetic distances between *O. polycarbonata*, other ploeotids (*L. corrugata* and *S. costata*), and *P. trichophorum* demonstrate that it is likely that these structural microtubules are highly conserved and have an early evolutionary origin within euglenids. Along these lines, because the microtubules that extend into the base of the feeding apparatus arise from the ventral root like the microtubules that form the MTR pocket in petalomonads (Yubuki & Leander, 2012), this configuration of supportive microtubules may even represent a component of the feeding apparatus that originated in the most recent common ancestor of all euglenids.

We have demonstrated that *O. polycarbonata* has a feeding apparatus that is more complex and robust than the feeding apparatuses previously observed in other ploeotids and is similar in organization and structure to the feeding apparatuses present in the Spirocuta (e.g.

P. trichophorum; *U. cyclostomus*). Contrasting the four-type system described by Triemer and Farmer (1991a), the overall structure of the feeding apparatus across euglenids is diverse and likely exists along a spectrum of complexity rather than fitting neatly into one of four categories (Lee & Simpson, 2014a). For example, some flexible phagotrophs have been reported to possess both an MTR pocket and a classical "Type III" feeding apparatus (Leander, Triemer, & Farmer, 2001), and several petalomonads (i.e. *Petalomonas hovassei* and *Calycimonas physaloides*) have been reported to possess a feeding apparatus with vanes but no associated rods (Kivic & Walne, 1984; Mignot, 1966; Triemer & Farmer, 1991a). Additional ultrastructural studies of phylogenetically distant phagotrophic species will provide the comparative context required to elucidate the diversity, complexity, and evolutionary history of the feeding apparatus across euglenids.

Flagellar apparatus

The flagellar apparatus of *O. polycarbonata* was consistent with previous ultrastructural studies of euglenids, such as the organization of the tripartite microtubular root system, the flagellar hairs, and the robust paraxonemal rods (Leander et al., 2017). The presence of a conspicuously thick ventral flagellum used for gliding motility in *O. polycarbonata* is shared with other ploeotids. Moreover, the electron-dense inclusion at the base of the ventral paraxonemal rod in *O. polycarbonata* is also present in a wide range of species across the Euglenida, including in the phagotrophs *Neometanema parovale*, *Serpenomonas costata*, *Entosiphon sulcatum*, and *Lentomonas corrugata* and in the phototroph *Eutreptiella pomquetensis* (Farmer & Triemer, 1988, 1994; Lee & Simpson, 2014a; Linton & Triemer, 1999; Triemer & Lewandowski, 1994). However, this electron-dense inclusion is rarely mentioned as an ultrastructural trait in previous studies, and its function is unknown.

Despite these similarities, there were also several novel traits or previously reported but poorly characterized traits associated with the flagellar apparatus in *O. polycarbonata*, such as two fibrous flagellar swellings, one present on each of the two paraxonemal rods. Various flagellar swellings that differ in structure and organization are present across euglenids: (1) the well-characterized paraxonemal body on the paraxonemal rod of the dorsal flagellum in phototrophic euglenids (Leander et al., 2017), (2) the paraflagellar swelling present on the axoneme of the dorsal flagellum in *Urceolus cyclostomus* (Leander et al., 2017; Leander, Triemer, & Farmer, 2001), (3) a fibrous swelling on the ventral paraxonemal rod of *N. parovale* (Lee & Simpson, 2014a), and (4) the swelling composed of striated material on the dorsal paraxonemal rod in *Peranema* and *Menoidium* (Hilenski & Walne, 1985; Leedale & Hibbard, 1974). No flagellar swellings have previously been reported in a ploeotid or petalomonad species, suggesting that this is the first occurrence of flagellar swelling in a taxon outside of the Spirocuta. Additionally, the condition of having two paraflagellar swellings, one on each flagellum, has never been reported in a euglenid until now.

The function of the two paraflagellar swellings in *O. polycarbonata* is unknown. The paraxonemal body in phototrophs facilitates photoreception and is generally well understood (Barsanti et al., 2012; Leander et al., 2017); however, the function of the paraflagellar swellings in the other taxa, which are all heterotrophic, is uncertain. It has been suggested that the paraflagellar swelling in *U. cyclostomus* might also function in photoreception, especially given the presence of a putative stigma (Leander, Triemer, & Farmer, 2001). If the paraflagellar swellings in *O. polycarbonata* facilitate photoreception as well, then this is accomplished in the absence of a stigma (i.e. shaded structure) and an expanded reservoir at the base of the flagellar pocket. It is unclear if all of the known paraflagellar swellings in different lineages of euglenids are homologous with one another due to important differences in ultrastructure, like their position relative to the axoneme and localization on the dorsal flagellum, the ventral flagellum or both. However, the organization of the paraflagellar swelling present on the dorsal paraxonemal rod of *O. polycarbonata* is similar to the paraxonemal body found in the Euglenophyceae. The uncertainty surrounding the overall diversity and function of paraflagellar swellings in phagotrophic euglenids provides an exciting avenue for further comparative research.

Does *O. polycarbonata* represent a cryptic species complex?

Different isolates of *O. polycarbonata* are consistently recovered as two monophyletic subgroups in molecular phylogenetic analyses of 18S rDNA sequences (Lax et al., 2019, 2021, 2023), and there is a significant amount of DNA divergence in this gene between these clades (87%–93% similarity) (Figure 8). Despite this divergence, there is no clear morphological difference in the isolated organisms across both clades when examined with light microscopy (Lax et al., 2019). *O. polycarbonata* might represent a cryptic species complex that could be split into two species in the future, and perhaps differences in the ultrastructure of isolates representing each subgroup will provide justification for the establishment of different species.

The ultrastructure for *L. corrugata* discussed here is based on the ultrastructural characterization of *L. applanatum* from Farmer and Triemer (1994). Cavalier-Smith (2016) formally declared *L. applanatum*, a junior synonym to *L. corrugata*, described by Larson and Patterson (1990), based on morphological similarity.

This revision was based on a comparison between light micrographs of *L. corrugata* obtained by Patterson and Simpson (1996) and scanning electron micrographs of *L. applanatum* from Farmer and Triemer (1994). No molecular data are available from either study for comparison and only Farmer and Triemer (1994) has ultrastructural data. More recently, Lax et al. (2019, 2021) determined the molecular phylogenetic placement of *L. corrugata* as a member of Alistosa, simultaneously rejecting a close relation to *Olkasia*. Unfortunately, no molecular data exist for *L. applanatum* from Farmer and Triemer (1994), and as such, it is impossible to confirm the molecular identity of *L. applanatum*. The ultrastructure of *L. applanatum* described by Farmer and Triemer (1994) exhibits more similarities to *O. polycarbonata* than with any member of Alistosa for which there is ultrastructural information, including taxa closely related to *L. corrugata*, such as *Decastava* and *Keelungia* (Cavalier-Smith et al., 2016; Chan et al., 2013). Therefore, we raise the possibility that *L. applanatum* from Farmer and Triemer (1994) and *L. corrugata* from Larson and Patterson (1990), Patterson and Simpson (1996) and Lax et al. (2019) are nonconspecific. Conversely, it is possible that the organism identified as *L. applanatum* in Farmer and Triemer (1994) might represent an undescribed relative of *Olkasia*, based on its ultrastructural similarity with *O. polycarbonata*. Additional ultrastructural studies for *Lentomonas* paired with molecular phylogenetic data are necessary to further examine the identity of this disputed taxon.

CONCLUSION

The ultrastructure of *O. polycarbonata* provides insights into the evolution of several cytoskeletal traits in euglenids associated with feeding and motility. The presence of a robust feeding apparatus that represents an intermediate state of complexity between the feeding apparatuses of ploeotids (e.g. *Serpenomonas costata*) and phagotrophic members of the Spirocuta (e.g. *U. cyclostomus*) is consistent with the molecular phylogenetic position of *O. polycarbonata* as the nearest sister lineage to the Spirocuta. Because *O. polycarbonata* appears to consume eukaryotic prey cells, perhaps a more robust arrangement of feeding rods and vanes helps facilitate the consumption of larger prey in the absence of a flexible pellicle. The existence of not one but two paraflagellar swellings, one per flagellum, demonstrates a new level of complexity associated with these enigmatic organelles across the Euglenida. Not only is the function of these swellings unclear in the various taxa that possess them, but the presence and diversity of these structures in other phagotrophic species remains unknown. Overall, when placed into a molecular phylogenetic context, improved knowledge of the ultrastructural diversity and complexity of the feeding and flagellar apparatuses in phagotrophic euglenids is expected to provide a rich source of evidence for reconstructing compelling patterns of character evolution in single-celled eukaryotes.

AUTHOR CONTRIBUTIONS

MVP and BSL conceived and guided the study. MVP collected the organisms and performed the microscopy within the context of her graduate studies research. MVP and RCM obtained the molecular data. MVP and GL performed molecular phylogenetic analyses. MVP and RCM made the figures. MVP wrote the first draft of the manuscript. MVP, RCM, GL, KCW, and BSL edited subsequent iterations of the manuscript. KCW and BSL funded the research.

ACKNOWLEDGMENTS

We wish to thank the UBC Bioimaging Facility (University of British Columbia) as well as the Akkeshi Marine Station (Hokkaido University) and the Electron Microscopy Facility in the Agricultural Department at Hokkaido University for the use of their facilities. We would also like to thank Siratee Riewluang and Shaun Cunningham from the Wakeman Laboratory for their assistance in field sample collection. Image acquisition and analysis for this project were conducted on the traditional, ancestral, and unceded territory of the xʷməθkʷəy̓əm (Musqueam) people. This work was funded by a grant to Kevin Wakeman through the Japanese Society for the Promotion of Science (No. 18K14774) and by a grant to BSL from the National Sciences and Engineering Research Council of Canada (NSERC 2019-03986).

CONFLICT OF INTEREST STATEMENT

None of the authors have a conflict of interest to disclose.

DATA AVAILABILITY STATEMENT

The data that supports the findings of this study are available in the supplementary material of this article.

ORCID

Maia V. Palka https://orcid.org/0009-0005-8743-4438

REFERENCES

Al-Qassab, S., Lee, W.J., Murray, S., Simpson, A.G.B. & Patterson, D.J. (2002) Flagellates from stromatolites and surrounding sediments in Shark Bay, Western Australia. *Acta Protozoologica*, 41, 91–144.

Barsanti, L., Evangelista, V., Passarelli, V., Frassanito, A.M. & Gualtieri, P. (2012) Fundamental questions and concepts about photoreception and the case of *Euglena gracilis*. *Integrative Biology*, 4, 22–36. Available from: https://doi.org/10.1039/c1ib00115a

Breglia, S.A., Yubuki, N., Hoppenrath, M. & Leander, B.S. (2010) Ultrastructure and molecular phylogenetic position of a novel euglenozoan with extrusive episymbiotic bacteria: *Bihospites bacati* n. gen. et sp. (Symbiontida). *BMC Microbiology*, 10, 145. Available from: https://doi.org/10.1186/1471-2180-10-145

Breglia, S.A., Yubuki, N. & Leander, B.S. (2013) Ultrastructure and molecular phylogenetic position of *Heteronema scaphurum*:

a eukaryovorous euglenid with a cytoproct. *The Journal of Eukaryotic Microbiology*, 60, 107–120. Available from: https://doi.org/10.1111/jeu.12014

Cavalier-Smith, T. (2016) Higher classification and phylogeny of euglenozoa. *European Journal of Protistology*, 56, 250–276. Available from: https://doi.org/10.1016/j.ejop.2016.09.003

Cavalier-Smith, T., Chao, E.E. & Vickerman, K. (2016) New phagotrophic euglenoid species (new genus *Decastava*; *Scytomonas saepesedens*; *Entosiphon oblongum*), Hsp90 introns, and putative euglenoid Hsp90 pre-mRNA insertional editing. *European Journal of Protistology*, 56, 147–170. Available from: https://doi.org/10.1016/j.ejop.2016.08.002

Chan, Y., Moestrup, O. & Chang, J. (2013) On *Keelungia pulex* nov. gen. et nov. sp., a heterotrophic euglenoid flagellate that lacks pellicular plates (Euglenophyceae, Euglenida). *European Journal of Protistology*, 49, 15–31. Available from: https://doi.org/10.1016/j.ejop.2012.04.003

David, V. & Archibald, J.M. (2016) Evolution: plumbing the depths of diplonemid diversity. *Current Biology*, 26, R1290–R1292. Available from: https://doi.org/10.1016/j.cub.2016.10.050

Edler, D., Klein, J., Antonelli, A. & Silvestro, D. (2020) raxmlGUI 2.0: a graphical interface and toolkit for phylogenetic analyses using RAxML. *Methods in Ecology and Evolution*, 12, 1–5. Available from: https://doi.org/10.1111/2041-210X.13512

Farmer, M.A. & Triemer, R.E. (1988) Flagellar systems in the euglenoid flagellates. *Biosystems*, 21, 283–291. Available from: https://doi.org/10.1016/0303-2647(88)90024-X

Farmer, M.A. & Triemer, R.E. (1994) An ultrastructural study of *Lentomonas applanatum* (Preisig) N. G. (Euglenida). *The Journal of Eukaryotic Microbiology*, 41, 112–119. Available from: https://doi.org/10.1111/j.1550-7408.1994.tb01482.x

Hilenski, L.L. & Walne, P.L. (1985) Ultrastructure of the flagella of the colorless phagotroph *Peranema trichophorum* (Euglenophyceae). II. Flagellar roots. *Journal of Phycology*, 21, 125–134. Available from: https://doi.org/10.1111/j.0022-3646.1985.00125.x

Katoh, K., Rozewicki, J. & Yamada, K.D. (2019) MAFFT online service: multiple sequence alignment, interactive sequence choice and visualization. *Briefings in Bioinformatics*, 20, 1160–1166. Available from: https://doi.org/10.1093/bib/bbx108

Kivic, P.A. & Walne, P.L. (1984) An evaluation of a possible phylogenetic relationship between the Euglenophyta and Kinetoplastida. *Origins of Life*, 13, 269–288. Available from: https://doi.org/10.1007/BF00927177

Kostygov, A.Y., Karnkowska, A., Votýpka, J., Tashyreva, D., Maciszewski, K., Yurchenko, V. et al. (2021) Euglenozoa: taxonomy, diversity and ecology, symbioses and viruses. *Open Biology*, 11, 200407. Available from: https://doi.org/10.1098/rsob.200407

Kuznicki, L., Mikolajczyk, E., Walne, P.L. & Hildebrand, E. (1990) Photobehavior of euglenoid flagellates: theoretical and evolutionary perspectives. *Critical Reviews in Plant Sciences*, 9, 343–369. Available from: https://doi.org/10.1080/07352689009382295

Larson, J. & Patterson, D.J. (1990) Some flagellates (Protista) from tropical marine sediments. *Journal of Natural History*, 24, 801–937. Available from: https://doi.org/10.1080/00222939000770571

Larsson, A. (2014) AliView: a fast and lightweight alignment viewer and editor for large datasets. *Bioinformatics*, 30, 3276–3278. Available from: https://doi.org/10.1093/bioinformatics/btu531

Lax, G., Cho, A. & Keeling, P.J. (2023) Phylogenomics of novel ploeotid taxa contribute to the backbone of the euglenid tree. *The Journal of Eukaryotic Microbiology*, 70, e12973. Available from: https://doi.org/10.1111/jeu.12973

Lax, G., Kolisko, M., Eglit, Y., Lee, W.J., Yubuki, N., Karnkowska, A. et al. (2021) Multigene phylogenetics of euglenids based on single-cell transcriptomics of diverse phagotrophs. *Molecular Phylogenetics and Evolution*, 159, 107088. Available from: https://doi.org/10.1016/j.ympev.2021.107088

Lax, G., Lee, W.J., Eglit, Y. & Simpson, A.G.B. (2019) Ploeotids represent much of the phylogenetic diversity of euglenids. *Protist*, 170, 233–257. Available from: https://doi.org/10.1016/j.protis.2019.03.001

Lax, G. & Simpson, A.G.B. (2013) Combining molecular data with classical morphology for uncultured phagotrophic euglenids (Excavata): a single-cell approach. *The Journal of Eukaryotic Microbiology*, 60, 615–625. Available from: https://doi.org/10.1111/jeu.12068

Leander, B.S. (2004) Did trypanosomatid parasites have photosynthetic ancestors? *Trends in Microbiology*, 12, 251–258.

Leander, B.S., Esson, H.J. & Breglia, S.A. (2007) Macroevolution of complex cytoskeletal systems in euglenids. *BioEssays*, 29, 987–1000.

Leander, B.S. & Farmer, M.A. (2000a) Epibiotic bacteria and a novel pattern of strip reduction on the pellicle of *Euglena helicoideus* (Bernard) Lemmermann. *European Journal of Protistology*, 36, 405–413. Available from: https://doi.org/10.1016/S0932-4739(00)80046-2

Leander, B.S. & Farmer, M.A. (2000b) Comparative morphology of the euglenid pellicle. I. Patterns of strips and pores. *The Journal of Eukaryotic Microbiology*, 47, 469–479. Available from: https://doi.org/10.1111/j.1550-7408.2000.tb00076.x

Leander, B.S. & Farmer, M.A. (2001) Comparative morphology of the euglenid pellicle. II. Diversity of strip substructure. *The Journal of Eukaryotic Microbiology*, 48, 202–217. Available from: https://doi.org/10.1111/j.1550-7408.2001.tb00304.x

Leander, B.S., Lax, G., Karnkowska, A. & Simpson, A.G.B. (2017) Euglenida. In: Archiblad, J.M., Simpson, A.G.B., Slamovits, C.H., Margulis, L., Melkonian, M., Chapman, D.J. et al. (Eds.) *Handbook of the protists*. Cham: Springer. Available from: https://doi.org/10.1007/978-3-319-32669-6_13-1

Leander, B.S., Triemer, R.E. & Farmer, M.A. (2001) Character evolution in heterotrophic euglenids. *European Journal of Protistology*, 37, 337–356. Available from: https://doi.org/10.1078/0932-4739-00842

Leander, B.S., Witek, R.P. & Farmer, M.A. (2001) Trends in the evolution of the euglenid pellicle. *Evolution*, 55, 2215–2235. Available from: https://doi.org/10.1111/j.0014-3820.2001.tb00737.x

Lee, W.J. & Simpson, A.G.B. (2014a) Ultrastructure and molecular phylogenetic position of *Neometanema parovale* sp. nov. (*Neometanema* gen. nov.), a marine phagotrophic euglenid with skidding motility. *Protist*, 165, 452–472. Available from: https://doi.org/10.1016/j.protis.2014.05.001

Lee, W.J. & Simpson, A.G.B. (2014b) Morphological and molecular characterisation of *Notosolenus urceolatus* Larsen and Patterson 1990, a member of an understudied deep-branching Euglenid group (Petalomonads). *The Journal of Eukaryotic Microbiology*, 61, 463–479. Available from: https://doi.org/10.1111/jeu.12126

Leedale, G.F. & Hibbard, D.J. (1974) Observations on the cytology and fine structure of the euglenoid genera *Menoidium* Perty and *Rhabdomonas* Fresenius. *Archiv für Protistenkunde*, 116, 319–345.

Linton, E.W. & Triemer, R.E. (1999) Reconstruction of the feeding apparatus in *Ploeotia costata* (Euglenophyta) and its relationship to other euglenoid feeding apparatuses. *Journal of Phycology*, 35, 313–324. Available from: https://doi.org/10.1046/j.1529-8817.1999.3520313.x

Mignot, J.P. (1966) Structure et ultrastructure de quelques Euglenomonadines. *Protistologica*, 2, 51–140.

Minh, B.Q., Schmidt, H.A., Chernomor, O., Schrempf, D., Woodhams, M.D., von Haeseler, A. et al. (2020) IQ-TREE 2: new models and efficient methods for phylogenetic inference in the genomic era. *Molecular Biology and Evolution*, 37, 1530–1534. Available from: https://doi.org/10.1093/molbev/msaa015

Montanaro, J., Gruber, D. & Leisch, N. (2016) Improved ultrastructure of marine invertebrates using non-toxic buffers. *PeerJ*, 31, e1860. Available from: https://doi.org/10.7717/peerj.1860

Nisbet, B. (1974) An ultrastructural study of the feeding apparatus of *Peranema trichophorum*. *The Journal of Protozoology*, 21, 39–48. Available from: https://doi.org/10.1111/j.1550-7408.1974.tb03614.x

Paerschke, S., Vollmer, A.H. & Preisfeld, A. (2017) Ultrastructural and immunocytochemical investigation of paramylon combined with new 18S rDNA-based secondary structure analysis clarifies phylogenetic affiliation of Entosiphon sulcatum (Euglenida: Euglenozoa). *Organisms, Diversity and Evolution*, 17, 509–520. Available from: https://doi.org/10.1007/s13127-017-0330-x

Patterson, D.J. & Simpson, A.G.B. (1996) Heterotrophic flagellates from coastal marine and hypersaline sediments in Western Australia. *European Journal of Protistology*, 32, 423–448. Available from: https://doi.org/10.1016/S0932-4739(96)80003-4

Simpson, A.G.B., Van den Hoff, J., Bernard, C., Burton, H.R. & Patterson, D.J. (1997) The ultrastructure and systematic position of the Euglenozoon *Postgaardi mariagerensis*, Fenchel et al. *Archiv für Protistenkunde*, 147, 213–225. Available from: https://doi.org/10.1016/S0003-9365(97)80049-8

Solomon, J.A., Walne, P.L. & Kivic, P.A. (1987) *Entosiphon sulcatum* (Euglenophyceae): flagellar roots of the basal body complex and reservior region. *Journal of Phycology*, 23, 85–98. Available from: https://doi.org/10.1111/j.1529-8817.1987.tb04430.x

Triemer, R.E. (1997) Feeding in *Peranema trichophorum* revisited (Euglenophyta). *Journal of Phycology*, 33, 649–654. Available from: https://doi.org/10.1111/j.0022-3646.1997.00649.x

Triemer, R.E. & Farmer, M.A. (1991a) The ultrastructural organization of the heterotrophic euglenids and its evolutionary implications. In: Patterson, D.J. & Larsen, J. (Eds.) *The biology of free-living heterotrophic flagellates*. Oxford: Clarendon Press, pp. 205–217.

Triemer, R.E. & Farmer, M.A. (1991b) An ultrastructural comparison of the mitotic apparatus, feeding apparatus, flagellar apparatus and cytoskeleton in euglenoids and kinetoplastids. *Protoplasma*, 164, 91–104. Available from: https://doi.org/10.1007/BF01320817

Triemer, R.E. & Fritz, L. (1987) Structure and operation of the feeding apparatus in a colorless euglenoid, *Entosiphon sulcatum*. *The Journal of Protozoology*, 34, 39–47. Available from: https://doi.org/10.1111/j.1550-7408.1987.tb03129.x

Triemer, R.E. & Lewandowski, C.L. (1994) Ultrastructure of the basal apparatus and putative vestigial feeding apparatuses in a quadriflagellate euglenoid (Euglenophyta). *Journal of Phycology*, 30, 1–159. Available from: https://doi.org/10.1111/j.0022-3646.1994.00028.x

Uhlig, G. (1964) Eine einfache Methode zur Extraktion der vagilen, mesopsammalen Mikrofauna. *Helgoländer Wissenschaftliche Meeresuntersuchungen*, 11, 178–185. Available from: https://doi.org/10.1007/BF01612370

Wolowski, K. (1995) *Dylakosoma pelophilum* Skuja, a rare colourless euglenophyte found in Poland. *Algological Studies*, 76, 75–78.

Yubuki, N., Edgcomb, V.P., Bernhard, J.M. & Leander, B.S. (2009) Ultrastructure and molecular phylogeny of *Calkinsia aureus*: cellular identity of a novel clade of deep-sea Euglenozoans with epibiotic bacteria. *BMC Microbiology*, 9, 16. Available from: https://doi.org/10.1186/1471-2180-9-16

Yubuki, N. & Leander, B.S. (2012) Reconciling the bizarre inheritance of microtubules in complex (Euglenid) microeukaryotes. *Protoplasma*, 249, 859–869. Available from: https://doi.org/10.1007/s00709-011-0340-z

SUPPORTING INFORMATION

Additional supporting information can be found online in the Supporting Information section at the end of this article.

How to cite this article: Palka, M.V., Manglicmot, R.C., Lax, G., Wakeman, K.C. & Leander, B.S. (2025) Ultrastructure of *Olkasia polycarbonata* (Euglenozoa, Euglenida) demonstrates cytoskeletal innovations associated with the feeding and flagellar apparatuses. *Journal of Eukaryotic Microbiology*, 72, e13074. Available from: https://doi.org/10.1111/jeu.13074